POLITECNICO DI TORINO
Repository ISTITUZIONALE

Transient field coupling and crosstalk in lossy lines with arbitrary loads

Terms of use:

Publisher copyright

(Article begins on next page)

30 April 2024

[21] *Operator's Manual Model 580 Micro-ohmmeter*, Document no. 580-900-01. Cleveland, OH: Keithley Instruments, Inc., Instrument Division, 1985.

[22] "Fabrication services," Mississippi State University to SPIRA Manufacturing Corporation, North Hollywood, CA, Purchase Order #923-04373, 1992.

[23] *Contact Shield Model 9101*. Smithfield, NC: Channel Master Electronic Lubricant, Division of Avnet, Inc., 1992.

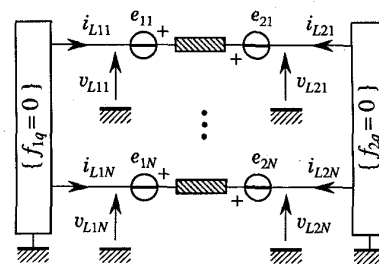
Fig. 1. Nonlinearly loaded transmission line: the relevant quantities for our formulation are indicated here and explained in the text.

Transient Field Coupling and Crosstalk in Lossy Lines with Arbitrary Loads

I. Maio and F. G. Canavero, *Member, IEEE*

Abstract— In this paper, we extend the transient scattering analysis of a lossy multiconductor transmission line to the evaluation of the interference produced by a field illuminating the line. The external interference is described by suitable voltage wave sources that are readily computed in the time domain and do not affect the structure of the transient scattering equations. The proposed formulation fully exploits the advantages of the transient analysis based on the line matched scattering parameters, dealing effectively with low-loss lines and helping the understanding of the interference mechanism through the physical interpretation of the results. The simplicity and efficiency of our approach is evidenced by means of a numerical example of the external interferences on a realistic nonlinearly loaded highly mismatched 3-conductor interconnect.

I. INTRODUCTION

Owing to the recent tendency toward decreasing rise times of the signal waveforms and toward higher frequency carriers, electromagnetic compatibility (EMC) is becoming a major concern in the design of many interconnections and wired communication systems. Moreover, an increasingly larger part of interconnects, at any size scale, behave as distributed structures and require transmission line (TL) models to account for the signal degradation caused by propagation. In consequence, a growing interest has developed for effective analysis schemes devoted to arbitrarily loaded multiconductor transmission lines (MTL's), possibly under the influence of a disturbing external field.

The coupling phenomenon of an external electromagnetic field to a transmission line (both two-conductor and multiconductor was extensively studied) and models using equivalent distributed voltage and current generators located along the line [1]–[4] are commonly employed. In the case of an electrical network with linear terminations, the analysis is effectively carried out in the frequency domain by means of a line characterization involving a proper set of parameters (e.g., see [5]). In the widely diffused case of nonlinear terminations, however, the analysis must be performed directly in the time domain, where, unfortunately, the characteristics of the transmission line and the evolution of the equivalent generators of the electromagnetic interference are usually particularly difficult to compute and handle.

The scattering parameter formulation, that offers relatively simple time characteristics also for the important case of low-loss (wideband)

TL's, established itself as a direct and effective method for the time-domain analysis of nonlinearly loaded MTL's (e.g., see [6]–[9]). In this paper, we extend the scattering formulation to the study of MTL's subjected to electromagnetic interferences, and we show that the effects of the external field can be handled by simply adding to the line ends proper source terms, which do not affect the structure of the solution algorithm, and thereby preserve all the advantages of the matched scattering formulation. Besides, the source terms for the matched scattering characterization are available for any field coupling formulation [4], have a particularly simple structure and can be readily calculated in the time domain. A numerical example is presented with the aim of showing that our formulation is an efficient and accurate method for studying the effects of interferences (due both to crosstalk and field coupling) on "long" interconnects that can be modeled as transmission lines.

In this paper, Section II and the Appendix are devoted to review the transient scattering equations of MTL's. In Section III the equivalent sources of the interfering field are evaluated and casted in a simple and computationally efficient form and, in Section IV, a simulation of the interference effects on a nonlinearly loaded 2-land PCB is presented.

Finally, it is worthwhile to clarify the notations that we use in this paper. Lower case letters represent time-domain variables and upper case letters indicate their counterparts in the domain of the complex frequency s, i.e., $x(t) \overset{\mathcal{L}_u^{-1}}{\underset{\mathcal{L}_u}{\rightleftharpoons}} X(s)$, and $\mathcal{L}_u$ denotes the Laplace transform operation. Also, the boldface character is used for the collections of elements, so that a indicates a time-varying vector or matrix and Y_{pq} is a scalar in the frequency domain.

II. SCATTERING TRANSIENT ANALYSIS OF MTL's

In this section, we review the scattering transient analysis of a loaded lossy MTL. The problem considered is defined in Fig. 1, where v_{Lpq} and i_{Lpq} ($p = 1, 2$ and $q = 1, \cdots, N$ throughout the paper) represent the load voltages and currents, respectively; the voltage sources e_{pq} at the line ends account for the system excitation, and the equations $f_{pq}(\{v_{Lpq}\}, \{i_{Lpq}\}) = 0$ (f_{pq} functions or operators) describe the behavior of the loads (linear or nonlinear).

The scattering parameter formulation is based on the representation of the electrical state of each network conductor in terms of wave variables. In the analysis of MTL problems, it is convenient to arrange voltages and currents as well as wave variables in vector form. For the problem of Fig. 1, the vector variables are obtained by collection of the scalar quantities of the same type defined in the same transverse section on the $N + 1$ conductors. For example, the vector of currents in the section of load no. 1 is $\boldsymbol{i}_{L1} = (i_{L11}, \cdots, i_{L1N})^T$, and
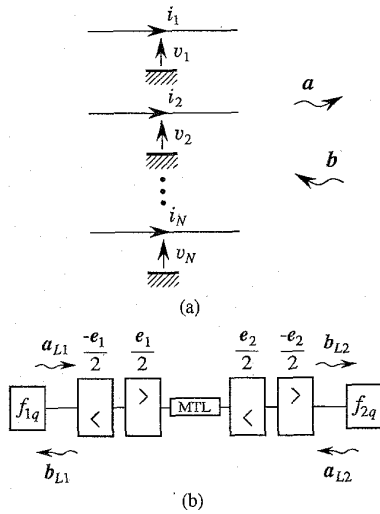
Fig. 2. (a) Conventions for voltages $v = (v_1, \cdots, v_N)^T$, currents $i = (i_1, \cdots, i_N)^T$, and voltage waves a and b in a generic section of the $(N+1)$-conductor structure. (b) Scattering diagram for the problem of Fig. 1.

the vector of sources at line end no. 2 is $e_2 = (e_{21}, \cdots, e_{2N})^T$ (T means matrix transposition). In this paper, the wave variables corresponding to voltages and currents at any transverse section of the structure are defined as

$$a = \tfrac{1}{2}(v + z * i)$$
$$b = \tfrac{1}{2}(v - z * i) \qquad (1)$$

where z is the transient characteristic impedance matrix of the MTL (i.e., the matrix converting a current traveling wave on the MTL into the corresponding voltage traveling wave) and $*$ denotes the convolution operator. The elements of vector a identify the signals propagating on the line in the direction of positive current flow [see Fig. 2(a)]. The wave variables a and b defined in (1) have dimensions of Volts and are called voltage waves. Other definitions of wave variables are possible: current waves, defined as $a^{(i)} = \tfrac{1}{2}(y * v + i)$, $b^{(i)} = \tfrac{1}{2}(y * v - i)$ with $Y = Z^{-1}$, are also used in transient problems, while power waves are typical of microwave applications [10]. The reason for adopting wave variables defined by the line characteristic admittance or impedance matrix, as done here, is that they lead to the matched scattering characterization of the MTL, and, in the widely diffused case of low-loss structures, this is preferable for the transient analysis and allows simpler expressions of the sources accounting for the external field interference (see next section).

The transient scattering equations of the system can be effectively written based on the scattering characteristics of the various network elements of Fig. 1. The scattering characterization is derived in the Appendix. A summary is given in Table I.

The combination of the scattering characteristics and the interpretation of the final equations is facilitated by a scattering diagram of the problem, indicating the scattering elements and their wave signals. The complete scattering diagram of the original problem is shown in Fig. 2(b). We introduce also the representation of the driving generators in terms of voltage wave sources, as discussed in the Appendix and described in Table II.

The transient equations for the load wave variables indicated in Fig. 2(b) follow by inspection, i.e.,

$$b_{L1} = h(-\mathcal{L}) * a_{L2} + \frac{e_2}{2} - \frac{e_1}{2}$$
$$b_{L2} = h(-\mathcal{L}) * a_{L1} + \frac{e_1}{2} - \frac{e_2}{2} \qquad (2)$$

TABLE I
SCATTERING CHARACTERISTICS OF NETWORK ELEMENTS

$$f_{1q}[a_{L1} + b_{L1}, \, y * (a_{L1} - b_{L1})] = 0$$
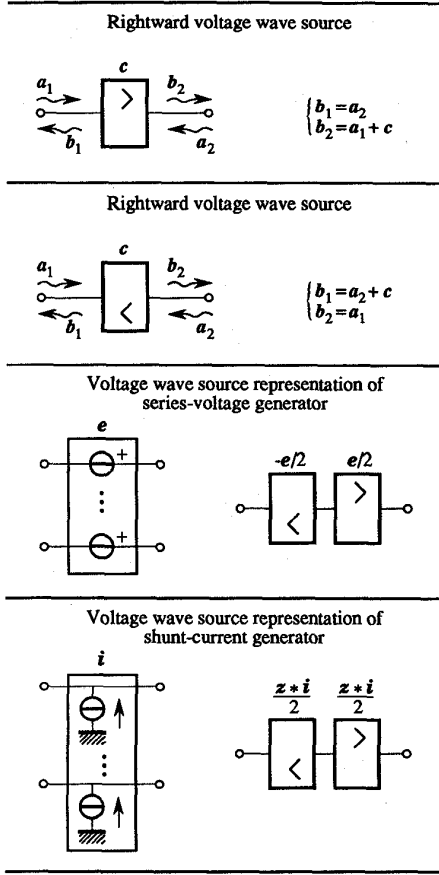$$f_{2q}[a_{L2} + b_{L2}, \, y * (a_{L2} - b_{L2})] = 0 \qquad (3)$$

where the matrix $h(\mathcal{L})$ is the transmission response of the matched MTL (i.e., the transient line propagation matrix) and is defined in the Appendix .

III. FIELD-COUPLING VOLTAGE WAVE SOURCES

In this section, we show that the interference effects caused by an electromagnetic field impinging on the MTL are readily accounted for by additional source terms included in the transient equations (2).

The effects of an external field on a TL can be modeled by suitable sets of voltage and currents generators distributed along the line and located at the line ends. Three different combinations of distributed and lumped generators can be used, which correspond to the three equivalent (although different) formulations proposed for the field-coupling process [1], [3], [4]. We then consider a MTL with a distribution of series voltage and shunt current generators and show their transformation into equivalent source terms that fit the model of Fig. 2. The diagrams of Fig. 3 illustrate the sequence of steps that are required for the evaluation of the scattering sources at the line ends. The process starts with infinitesimal voltage and current generators located on each wire of the line, at an arbitrary section z [Fig. 3(a)]. These generators translate the effects of an external interfering electromagnetic field, and their presence depends on the field coupling formulation adopted: they are both present in case of a "balanced" formulation [1], while the current source is absent in case of the "electric-field" formulation [3], and the voltage source is omitted by the "magnetic-field" formulation [4]. The conversion of voltage and current sources into voltage wave generators is readily accomplished by means of the schemes of Table II, explained in the Appendix [see Fig. 3(b)]. The voltage wave generators are then moved from the arbitrary section z to the end of the line: this

TABLE II
VOLTAGE WAVE SOURCES

Rightward voltage wave source

$\begin{cases} b_1 = a_2 \\ b_2 = a_1 + c \end{cases}$

Rightward voltage wave source

$\begin{cases} b_1 = a_2 + c \\ b_2 = a_1 \end{cases}$

Voltage wave source representation of
series-voltage generator

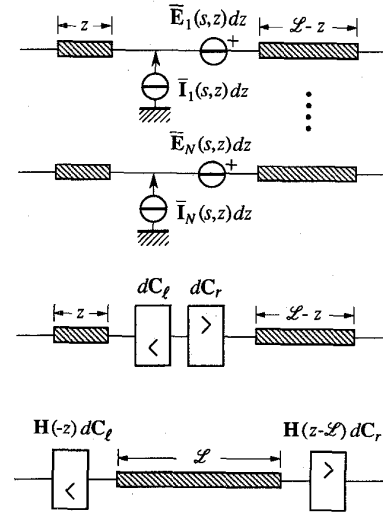Voltage wave source representation of
shunt-current generator

Fig. 3. Voltage wave generators equivalent to the infinitesimal shunt-current and series-voltage generators induced in the generic section z of the line. The original current and voltage generators are shown in (a), their equivalent voltage wave sources (for reference impedance Z) in (b), where $dC_{\binom{\ell}{r}} = \frac{1}{2}[Z\overline{I}(s, z)\binom{-}{+}\overline{E}(s, z)]\,dz$, and the equivalent voltage wave sources at the line ends in (c).

implies the use of the transfer function of the matched MTL, H [see Fig. 3(c)]. The three-step procedure of Fig. 3 must be repeated for all line sections, and the result is obtained by integration of all contributions along the line. This yields

$$B_{f1} = \frac{1}{2} \int_0^{\mathcal{L}} H(-z)[Z\overline{I}(s, z) - \overline{E}(s, z)]\,dz \qquad (4)$$

$$B_{f2} = \frac{1}{2} \int_0^{\mathcal{L}} H(z - \mathcal{L})[Z\overline{I}(s, z) + \overline{E}(s, z)]\,dz. \qquad (5)$$

The above integral contributions can be interpreted as two extra sources to be added at the line ends in the scheme of Fig. 2. Correspondingly, (2) are completed with the field coupling terms, and become

$$b_{L1} = h(-\mathcal{L}) * \left(a_{L2} + \frac{z * i_2 + e_2}{2} \right)$$
$$+ \frac{z * i_1 - e_1}{2} + b_{f1}$$

$$b_{L2} = h(-\mathcal{L}) * \left(a_{L1} + \frac{z * i_1 + e_1}{2} \right)$$
$$+ \frac{z * i_2 - e_2}{2} + b_{f2} \qquad (6)$$

where the driving generators at the line ends e_p, i_p include the effects of the possible field-induced terminal generators.

Our derivation of the source terms (4) and (5) is formally equivalent to the Green function method used in [11] to compute the circuit response of a linearly loaded line to an external field. In fact, B_{fp} are

the voltage wave response of the MTL terminated on matched loads and the transmission operators of the MTL, $H(-z)$, $H(z - \mathcal{L})$, are the Green functions between any section z and the line ends. When nonlinear loads are considered, however, closed form expressions of the circuit response cannot be obtained and the source terms (4) and (5) offer the simplest possible characterization of the influence of an external field. In contrast with other possible field-coupling equivalent sources (e.g., the line Thévénin generators of [12]), (4) and (5) are free from multiple reflection resonances and their simplicity facilitates the evaluation and representation of their transient expression to be used in (6). Besides, the simplicity of the expressions of the field-coupling voltage-wave sources allows us to construct the line impulse responses to the external field. Such functions are useful for the solution of closed loop problems, where the external field is produced by the transient on the MTL (e.g., consider a power device inducing an electromagnetic field on the interconnects of its low-level driving circuit). Finally, the expressions of the voltage wave sources, highlighting the physical mechanism of the field coupling, help to study the sensitivity of the MTL to the external interference. In fact, for a simple two-conductor line where $H(z) = \exp(-\gamma z)$, (4) and (5) can be interpreted as the Laplace transform of the spatial distributions of the equivalent generators.

In the important case of a plane-wave interfering field, the spatial integration in the field-coupling sources (4) and (5) can be carried out analytically. For the following explicit calculations, we refer to the field-coupling formulation that makes use of scattered voltages and total currents [3]. This formulation models the field effect with a continuous distribution of voltage generators proportional to the field component parallel to the line, and two terminal voltage generators depending on the transverse field component at the line ends. The impinging plane wave is defined by its propagation unit vector $\hat{n}$ and its electric field polarization unit vector $\hat{p}$. The geometry of the problem is shown in Fig. 4, where the angle θ is defined between the unit vectors $\hat{x}$ and $\hat{n}$, and the angle ψ between $\hat{z}$ and the projection of $\hat{n}$ on the (y, z) plane. The expression of $\overline{E}$ takes the form [12]

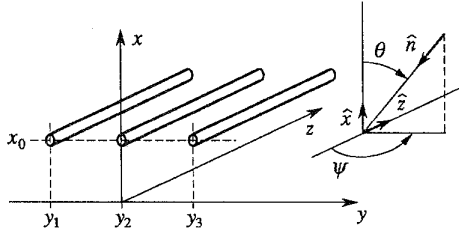$$\overline{E}(s, z) = G(s)E(s)e^{-\gamma_0 z}, \qquad (7)$$

Fig. 4. Geometry of the multiconductor transmission line illuminated by an external interfering field; $\hat{n}$ is the propagation unit vector of the impinging plane wave, and θ and ψ are its characteristic angles.

where $E(s)$ is the spectrum of the interfering signal, $\gamma_0 = (s/v_0)\hat{n} \cdot \hat{z} = s \sin\theta \cos\psi / v_0$ is the propagation function in the z direction of the plane wave (v_0 is the speed of light in the medium), and $G(s)$ contains transfer functions depending on the geometry and losses of the guiding structure. For the above form of $\overline{E}(s, z)$, (4) becomes

$$B_{f1} = -\frac{1}{2}\int_0^{\mathcal{L}} H(-z)G(s)E(s)e^{-\gamma_0 z}\,dz$$
$$= -\frac{1}{2}\left[\int_0^{\mathcal{L}} H(-z)e^{-\gamma_0 z}\,dz\right]G(s)E(s) \qquad (8)$$

where the current contribution is not present [i.e., $\overline{I}(s, z) = 0$], due to formulation adopted. Since the matrix of voltage modal profiles is independent of z, the integral of (8) can be computed separately for any modal propagation factor, i.e.,

$$B_{f1} = -\frac{1}{2}M_V \, \text{diag}\left\{\int_0^{\mathcal{L}} e^{-(\gamma_k + \gamma_0)z}\,dz\right\}$$
$$\cdot M_V^{-1}G(s)E(s)$$
$$= -\frac{1}{2}M_V \, \text{diag}\left\{\frac{1 - e^{-(\gamma_k + \gamma_0)\mathcal{L}}}{\gamma_k + \gamma_0}\right\}$$
$$\cdot M_V^{-1}G(s)E(s). \qquad (9)$$

This expression can be simplified by factorizing the propagation matrix of the line:

$$B_{f1} = -\frac{1}{2}M_V \, \text{diag}\left\{\frac{1}{\gamma_k + \gamma_0}\right\} M_V^{-1}G(s)E(s)$$
$$+ \frac{1}{2}M_V \, \text{diag}\{e^{-\gamma_k\mathcal{L}}\} \, \text{diag}\left\{\frac{1}{\gamma_k + \gamma_0}\right\}$$
$$\cdot M_V^{-1}G(s)E(s)e^{-\gamma_0\mathcal{L}}$$
$$= -\frac{1}{2}[1 - H(-\mathcal{L})e^{-\gamma_0\mathcal{L}}]M_V \, \text{diag}\left\{\frac{1}{\gamma_k + \gamma_0}\right\}$$
$$\cdot M_V^{-1}G(s)E(s). \qquad (10)$$

The field-coupling voltage wave source B_{f2} at the other line end can be treated similarly, and results

$$B_{f2} = \frac{1}{2}[e^{-\gamma_0\mathcal{L}} - H(-\mathcal{L})]$$
$$\cdot M_V \, \text{diag}\left\{\frac{1}{\gamma_k - \gamma_0}\right\} M_V^{-1}G(s)E(s). \qquad (11)$$

The inclusion of field-coupling voltage wave sources into (6) can be simplified, based on a different arrangement of (10) and (11) and on an interpretation similar to the one shown in Fig. 3. In fact, it is evident that B_{f1} is equivalent to a leftward voltage wave source

$$\overline{B}_{f1} = -\frac{1}{2}M_V \, \text{diag}\left\{\frac{1}{\gamma_k + \gamma_0}\right\} M_V^{-1}G(s)E(s) \qquad (12)$$

located at line end no. 1, plus a leftward voltage wave source

$$\overline{A}_{f2} = \frac{1}{2}M_V \, \text{diag}\left\{\frac{1}{\gamma_k + \gamma_0}\right\} M_V^{-1}G(s)E(s)e^{-\gamma_0\mathcal{L}} \qquad (13)$$

located at line end no. 2. Similarly, B_{f2} is split into two rightward voltage wave generators at the two line ends, i.e.,

$$\overline{A}_{f1} = -\frac{1}{2}M_V \, \text{diag}\left\{\frac{1}{\gamma_k - \gamma_0}\right\} M_V^{-1}G(s)E(s) \qquad (14)$$

$$\overline{B}_{f1} = \frac{1}{2}M_V \, \text{diag}\left\{\frac{1}{\gamma_k - \gamma_0}\right\} M_V^{-1}G(s)E(s)e^{-\gamma_0\mathcal{L}}. \qquad (15)$$

The new sources $\overline{A}_{fp}$ and $\overline{B}_{fp}$ are free from the line propagation matrix and can be easily inverse-transformed and included in the system of transient equations. Moreover, this arrangement avoids the numerical noise that can occur for some incidence directions and field polarizations, if field-coupling sources computed by direct inversion of (10) and (11) are used in the transient equations. In fact, noisy numerical results can arise from the computation, because the b_{fp} values are summed in (6) with similar contributions originating at the other line end but obtained by convolution with the transient line propagation matrix.

In summary, the complete transient equations for the network of Fig. 1 interfered by a plane wave are

$$b_{L1} = h(-\mathcal{L}) * \left(a_{L2} + \frac{e_2 - v_2'}{2} + \overline{a}_{f2}\right)$$
$$+ \frac{v_1' - e_1}{2} + \overline{b}_{f1}$$
$$b_{L2} = h(-\mathcal{L}) * \left(a_{L1} + \frac{e_1 - v_1'}{2} + \overline{a}_{f1}\right)$$
$$+ \frac{v_2' - e_2}{2} + \overline{b}_{f2}$$
$$f_{pq}[a_{Lp} + b_{Lp}, \, y * (a_{Lp} - b_{Lp})] = 0 \qquad (16)$$

where v_p' are the vectors of voltage generators at the line ends accounting for the field component transverse to the line [12].

IV. NUMERICAL EXAMPLE

The proposed approach to the evaluation of interferences on MTL's was extensively validated against a conventional frequency domain analysis tool [5], [12] applied to structures with linear loads: the results of the two approaches are in perfect agreement, but not shown here for brevity. We concentrate, however, on the discussion of the interference effects in a realistic nonlinearly loaded interconnect.

A. Circuit and Models

The circuit of this example is described in Fig. 5, where an asymmetric 2-land PCB, driven and loaded by inverter gates, is exposed to an impinging plane wave with a biexponential time envelope, whose expression is

$$\vec{\mathcal{E}}(t, \vec{r}) = \hat{p}\mathcal{A}(e^{-t'/t_1} - e^{-t'/t_2}), \quad t' = t - \frac{\hat{n} \cdot \vec{r}}{v_o} \qquad (17)$$

where $\vec{r}$ is the position vector in the reference frame of Fig. 5, $\mathcal{A}$ is a dimensional constant, and t_1, t_2 are time constants. The reference conductor (ideal) of the MTL coincides with the (y, z) plane and the two lands (of widths w_1 and w_2, and of thickness d) lie along the z axis at $(x_o, \pm\Delta y/2)$, where x_o is the thickness of the dielectric substrate (see Fig. 5 and the parameter values of Table III). The driving inverters are assumed to be in the HIGH logical state and are modeled by a two-segment static characteristic in parallel with a capacitor of 1 pF, whereas the receiving inverters are modeled with the sole capacitor of 1 pF (see [13]). The two-segment characteristic is described by the following Thévenin equivalent:

$$E_{eq} = 4\,\text{V},$$
$$R_{eq} = \begin{cases} 40\,\Omega, & v_{L1p} < 4\,\text{V} \\ 450\,\Omega, & v_{L1p} \geq 4\,\text{V}. \end{cases} \qquad (18)$$

TABLE III
PARAMETER VALUES OF THE EXAMPLE

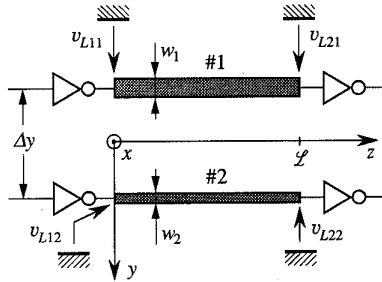| Interfering plane wave parameters (see (17))	
$\mathcal{A}$	10^4 V/m
t_1	10^{-8} s
t_2	10^{-9} s
θ	45°
ψ	60°
$\hat{p} \cdot \hat{x}$	0
Geometrical and electrical characteristics of the line (see Fig. 5)	
$\mathcal{L}$	0.25 m
Δy	150 μm
x_o	200 μm
w_1	60 μm
w_2	30 μm
d	30 μm
ϵ_r substrate	9
σ strip	5.6×10^7 m$^{-1}\Omega^{-1}$
Line parameters	
$R_{DC,1}$	10 Ω
$R_{DC,2}$	20 Ω
τ_1	1.27 ns
τ_2	1.44 ns

Fig. 5. Top view of the circuit of the numerical example developed in Section IV. It consists of a low-loss asymmetric 2-land PCB loaded by inverters. The two driving inverters at $z = 0$ are in the HIGH state and are represented by a nonlinear equivalent [see (18) in the text], while the receivers at $z = \mathcal{L}$ are simple 1-pF capacitors. The values of the geometrical and electrical parameters of the line, and of the interfering wave are given in Table III.

The transfer functions $G = [G_1(s), G_2(s)]^T$ for the distributed voltage generators [see (7)] are obtained from the primary electric field [12] in the stratified dielectric medium, i.e.,

$$G_{\binom{1}{2}} = 2 \sin \psi \cos \theta x_o \frac{s}{v_o}$$

$$\cdot \left(1 \mp \frac{\Delta y}{2} \sin \psi \sin \theta \frac{s}{v_o}\right) \quad (19)$$

where the electric field is assumed to be contained in the (y, z) plane, and the approximations allowed by the condition of a slowly varying disturbing field (i.e., $t_{1,2} \gg x_o/v_o$, $\Delta y/v_o$) are also exploited.

The source terms and the line transient characteristics needed in the system transient equations (16) are obtained by numerical inverse Laplace Transform [14] of the corresponding frequency functions. In particular, the sources $\overline{A}_{fp}$, $\overline{B}_{fp}$ are obtained by means of the inverse transformation of (12)–(15), whereas h and y come from the inverse transformation of (see Appendix)
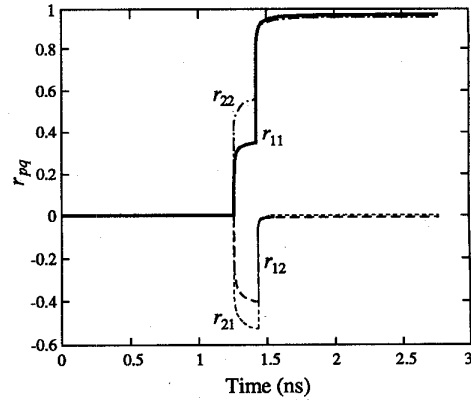
$$H = M_V \text{ diag} \{e^{\gamma_k \mathcal{L}}\} M_V^{-1}$$

Fig. 6. Transmission step responses $r_{pq} = \int_0^t h_{pq} \, dt'$ for the 3-conductor TL of the example discussed in Section IV.

$$Y = \overline{Y} M_V \text{ diag} \left\{\frac{1}{\gamma_k}\right\} M_V^{-1}. \quad (20)$$

The MTL is assumed of RLC type, i.e., $\overline{Z} = R(s)+sL$ and $\overline{Y} = sC$, where R, L, and C are the per-unit-length resistance, inductance and capacitance matrices of the guiding structure, respectively. The resistance matrix is assumed of the form $R(s) = \text{diag}\{R_q\}$, and its elements are approximated as in [15], i.e.,

$$R_q(s) = \frac{R_{o,q}\sqrt{2s}}{1 - \exp\left\{-\frac{R_{o,q}\sqrt{2s}}{R_{DC,q}}\right\}}, \quad (21)$$

where $R_{DC,q}$ and $R_{o,q}\sqrt{2s}$ are the per-unit-length DC and high-frequency skin effect resistances [16] of each copper strip, respectively. This resistance model is one of the simplest available for rectangular conductors, yet it is fairly adequate for the considered example, because in the simulation band of interest the line impulse responses are mainly determined by skin losses. If needed, more accurate resistance models can be handled by the numerical inversion of Laplace Transform for a negligible additional computational cost.

The transmission step responses $r_{pq} = \int_0^t h_{pq} \, dt'$ for the structure under analysis are shown in Fig. 6. The reason for using such step responses is that they are easier to represent than the impulse responses h_{pq}. The differences between the step responses of the same type in Fig. 6 arise from the longitudinal asymmetry of the MTL. For this example, the convolution integrals of the transient scattering equations (16) are computed by representing the unknown variables as piecewise linear functions with nonuniformly spaced time samples and by a summation formula involving the step responses and their integrals (e.g., see [17]). Although the cost of this method is proportional to the square of the number of time steps, it is suited for testing purposes, since it offers accurate and reliable results.

Finally, it should be emphasized that the asymmetry of the line is aimed at showing the feasibility of the proposed approach in the most general case of MTL structures with frequency dependent modal profiles. However, for practical applications, in most low-loss MTL's (included the one of the example) the frequency dependent modal profiles can be approximated by the constant modal profiles of the lossless structure, without appreciable errors in the transient evolution but with large computational savings.

B. Numerical Results

The end voltages v_{Lpq} obtained with our formulation for the problem of Fig. 5 are shown in Fig. 7, where the time behavior and
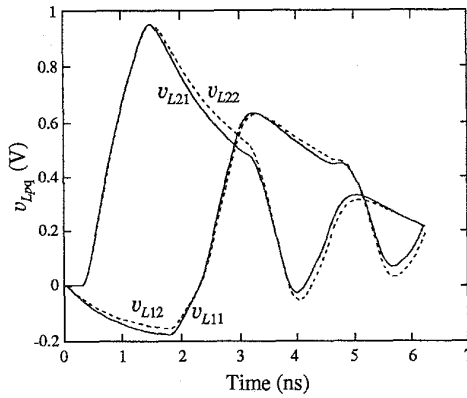
Fig. 7. Transient end voltages v_{Lp1} (solid curves) and v_{Lp2} (dotted curves) due to a plane-wave interference on the transmission line loaded by inverters and shown in Fig. 5.
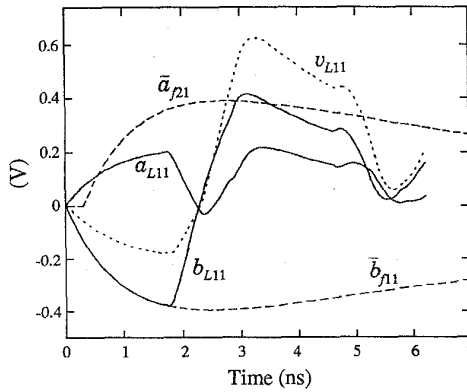

Fig. 8. Decomposition of the v_{L11} waveform of Fig. 7 (dotted curve) in terms of the transient voltage waves a_{L11} and b_{L11} (solid curves). Also, the source terms $\bar{b}_{f11}$ and $\bar{a}_{f21}$ (dashed curves) are shown. In the text, it is illustrated how these quantities can help in the physical interpretation of the results.

levels of the noise induced into the electronic system are represented. The differences between the responses of the two lands are mainly due to their asymmetry, because the external excitation is nearly symmetric (i.e., $\bar{a}_{fp1} \approx \bar{a}_{fp2}$ and $\bar{b}_{fp1} \approx \bar{b}_{fp2}$, due to the small phase difference of the field on the two conductors) and the line drivers and loads are symmetric. From the EMC point of view, this example points out the insensitivity of the structure under study to the external disturbances, since the signals induced on the line are on the order of 1 V, for a peak electric field of 10^4 V/m. The immunity of the structure is mainly controlled by the distance x_o of the signal conductors from the reference conductor: this distance, that appears as a multiplicative factor in G_q terms [see (19)], is very small in the structure considered. Significant disturbances can be produced by moderate external fields in structures that have x_o values on the order of 10^{-2} m and larger, like wired interconnects and communication cables.

The above example is well suited to evidence an important advantage of our formulation, i.e., its ability to provide an interpretation of the output waveforms, by shading light on the propagation mechanisms of the external interferences. This is obtained by the adoption of the voltage waves, that have an intrinsic physical meaning, and by the form of the external interference generators given at the end of Section III. For example, the v_{L11} signal shown in Fig. 7 is
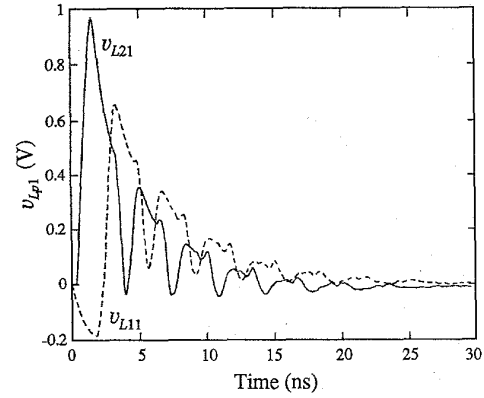

Fig. 9. Long-time evolution of the v_{L11} and v_{L21} waveforms.

readily verified and interpreted with the help of Fig. 8, where the component voltage waves a_{L11}, b_{L11}, and the voltage wave sources $\bar{a}_{f21}$, $\bar{b}_{f11}$, which are attenuated and slightly distorted replicas of the field biexponential waveform, are shown.

The voltage wave generators $\bar{a}_{f21}$, $\bar{b}_{f11}$ are the only sources for this example, since the v'_{pq} terms are absent due to $\hat{p} \cdot \hat{x} = 0$. The interpretation of the features of Fig. 8 is then straightforward. In particular, the 0.3 ns-delay of the field contribution at line end no. 2 ($\bar{a}_{f21}$) is caused by the angle of incidence of the interfering wave; the initial contribution to b_{L11} coincides with the source term $\bar{b}_{f11}$ at the same line end, until the contributions of $\bar{a}_{f2q}$ reaches end no. 1 (in fact, the "even mode" propagation delay is $\tau_2 \approx$ 1.44 ns); the jump from the 40-Ω branch of the nonlinear load characteristic to the other branch is evident for $t \approx 2.3$ ns (in fact, at such instant, the instantaneous reflection coefficient becomes positive, since v_{L11} becomes larger than 4 V). It should be pointed out that such detailed physical interpretation of the transient signals is useful for a qualitative analysis of the circuit behavior: in fact, it can help the designer to track the interference sources and derive bounds for the interference levels.

The long-time evolution of the waveforms v_{Lp1} is finally represented in Fig. 9, in order to show the good stability properties of the proposed approach.

V. CONCLUSION

In this paper, we extend the scattering transient analysis of lossy MTL's to include the interference effects produced by an external electromagnetic field. The advantages of the transient scattering formulation, i.e., its ability to handle effectively low-loss lines and its physical meaning are fully exploited. The extension is based on voltage wave sources depending on the field coupling, that are directly derived in the scattering parameter framework. Such equivalent scattering sources are readily available for any field coupling formulation and have a simple structure, that makes easier the evaluation of their transient expressions. Besides, their physical meaning provides insight in the interference process and helps both the validation of simulation results and the construction of worst-case rules for circuit qualitative analysis.

The efficiency and accuracy of the proposed approach is demonstrated in the numerical example of Section IV, where a realistic nonlinearly loaded highly mismatched two-conductor interconnect is examined and the results are produced in a matter of minutes on a personal computer, for an implementation in an interpreted programming language. The structure of the formulation is also

suitable for the implementation in standard circuit simulators, thus increasing the potential of such tools.

APPENDIX

In this Appendix, we derive the scattering characteristics of the elements of the distributed network of Fig. 1. For simplicity, frequency-domain notation is used wherever possible. The discussion is carried out for the general case of an $(N+1)$-conductor line (of course, $N = 1$ refers to a two-conductor line). The results are collected in Tables I and II.

A. Transmission Line Section

The scattering description of a two-sided network is

$$\begin{pmatrix} B_1 \\ B_2 \end{pmatrix} = S \begin{pmatrix} A_1 \\ A_2 \end{pmatrix}$$
$$= \begin{pmatrix} S_{11} & S_{21} \\ S_{21} & S_{11} \end{pmatrix} \begin{pmatrix} A_1 \\ A_2 \end{pmatrix} \tag{22}$$

where B_1 and B_2 represent the scattered voltage waves at the ports (possibly more than one) on sides no. 1 and 2, respectively; A_1 and A_2 are the corresponding impinging voltage waves.

There are several ways to obtain the scattering parameter matrices S_{11}, S_{12}, S_{21}, S_{22} for a MTL (e.g., see [6]). We obtain them by exploiting their relationships with the line voltages and currents, i.e.,

$$A_p = \tfrac{1}{2}(V_p + ZI_p)$$
$$B_p = \tfrac{1}{2}(V_p - ZI_p), \quad p = 1, 2. \tag{23}$$

In fact, the vectors of voltage $V(z)$ and current $I(z)$ distributions along the MTL have the following structure:

$$V(z) = H(-z)V^+ + H(z)V^-$$
$$I(z) = Y[H(-z)V^+ - H(z)V^-] \tag{24}$$

where V^+, V^- are constant vectors determined by the line boundary conditions, Y is the line characteristic admittance matrix, $H(z) = M_V \operatorname{diag}\{e^{\gamma_k z}\}M_V^{-1}$ is the line propagation matrix, M_V is the matrix of voltage modal profiles, γ_k are the modal propagation constants, and the z axis is assumed to originate at line end no. 1 and directed toward line end no. 2. The matrix of voltage modal profiles and the modal propagation constants are solutions of the eigenvalue problem

$$\overline{Z}\,\overline{Y}M_V = M_V \operatorname{diag}\{\gamma_k^2\} \tag{25}$$

where $\overline{Z}$ and $\overline{Y}$ are the per-unit-length line impedance and admittance matrices, respectively.

If we consider the TL diagram in the first row of Table I, we can substitute (24) in (23), obtaining the following relations in matrix form:

$$\begin{pmatrix} B_1 \\ B_2 \end{pmatrix} = \begin{pmatrix} 0 & 1 \\ H(-\mathcal{L}) & 0 \end{pmatrix} \begin{pmatrix} V^+ \\ V^- \end{pmatrix} \tag{26}$$

$$\begin{pmatrix} A_1 \\ A_2 \end{pmatrix} = \begin{pmatrix} 1 & 0 \\ 0 & H(\mathcal{L}) \end{pmatrix} \begin{pmatrix} V^+ \\ V^- \end{pmatrix}. \tag{27}$$

The steps necessary for the computation of A_1 are shown for example, i.e.,

$$A_1 = \frac{1}{2}(V_1 + ZI_1)$$
$$= \tfrac{1}{2}[V(z = 0) + ZI(z = 0)]$$
$$= \tfrac{1}{2}[V^+ + V^- + ZY(V^+ - V^-)]$$
$$= V^+ \tag{28}$$

where, of course, $ZY = 1$

The substitution of (26) and (27) into the left- and right-hand side of (22) yields an expression for the scattering super-matrix S, i.e.,

$$S = \begin{pmatrix} 0 & 1 \\ H(-\mathcal{L}) & 0 \end{pmatrix} \begin{pmatrix} 1 & 0 \\ 0 & H(\mathcal{L}) \end{pmatrix}^{-1}$$
$$= \begin{pmatrix} 0 & H(-\mathcal{L}) \\ H(-\mathcal{L}) & 0 \end{pmatrix} \tag{29}$$

where $H^{-1}(\mathcal{L}) = H(-\mathcal{L})$ has been used.

Finally, the matched scattering characteristic of the MTL in the time domain is

$$\begin{pmatrix} b_1 \\ b_2 \end{pmatrix} = \begin{pmatrix} 0 & h(-\mathcal{L}) \\ h(-\mathcal{L}) & 0 \end{pmatrix} \begin{pmatrix} a_1 \\ a_2 \end{pmatrix}. \tag{30}$$

$$h(-\mathcal{L}) = \mathcal{L}_u^{-1}[M_V \operatorname{diag}\{e^{-\gamma_k \mathcal{L}}\}M_V^{-1}]. \tag{31}$$

The scattering characteristics for a general (nonmatched) reference impedance matrix can be obtained similarly. In such a case, the relations between the voltage waves and the solution constants of (26) and (27) are represented by full matrices involving the reflection coefficient between the selected reference impedance and the line characteristic impedance. However, in this paper we limit our discussion to the matched scattering characteristics since, in the widely diffused case of low-loss lines, the transient expressions of the nonmatched scattering parameters contain multiple peaks and are difficult to compute and represent.

B. Lumped Loads

The load scattering characteristics are simply obtained by substituting v and i in the load characteristic in terms of the voltage wave variables a and b. The resulting equations $f_q[a + b, y * (a - b)] = 0$ (second row of Table I) are used to compute the voltage wave a reflected by the load, for a known impinging voltage wave b. It should be remarked that we express the load equations by means of the transient characteristic admittance, because $y(t)$ has finite asymptotic values also for the RLC TL [18], which is the most common interconnect model. For the same reason, current waves rather than voltage waves should be used in RLC lines, since they are defined for steady state ($s = 0$) problems, too. Voltage waves are used in this paper instead, because we assume they are more familiar to the reader.

C. Lumped Sources

The scattering representation in the third row of Table I follows from (23), by means of the definition of the ideal series voltage source, i.e.,

$$B_1 = \tfrac{1}{2}(V_1 - ZI_1)$$
$$= \tfrac{1}{2}(V_2 - E + ZI_2)$$
$$= A_2 - \frac{E}{2}$$
$$B_2 = \tfrac{1}{2}(V_2 - ZI_2)$$
$$= \tfrac{1}{2}(V_1 + E + ZI_1)$$
$$= A_1 + \frac{E}{2}. \tag{32}$$

Also, we found useful the definition of voltage wave sources as in the first and second rows of Table II. They are elements transparent to the voltage waves impinging on them and simply add their signal to the output voltage wave propagating in the direction of the arrow. Voltage wave sources allow a unified representation of voltage and current generators and help in the evaluation of the scattering characteristics of complex nonautonomous networks (e.g., see Section III). The last two rows of Table II show the use of voltage

IEEE TRANSACTIONS ON ELECTROMAGNETIC COMPATIBILITY, VOL. 37, NO. 4, NOVEMBER 1995
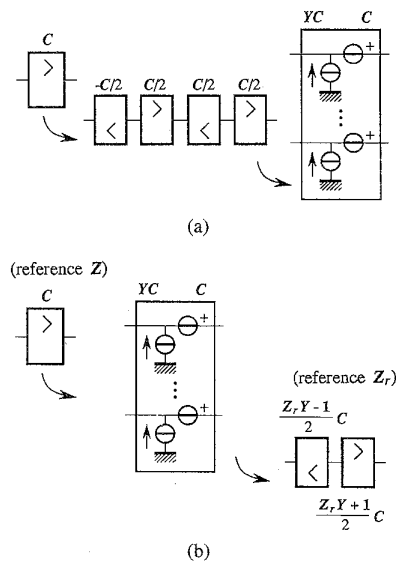

Fig. 10. Electric equivalent of the "voltage wave source" block. In (a), a circuit equivalent is derived, and in (b) it is used to convert a voltage wave source C, defined for the characteristic reference impedance Z, to the case of an arbitrary reference impedance Z_r.

wave sources to represent the series voltage generators and the shunt current generators. The equivalence shown in row 3 of Table II is obtained by direct comparison of the scattering characteristics of row 3 of Table I with rows 1 and 2 of Table II. The equivalence for the current generators follows similarly.

In Fig. 10(a) it is also shown that the voltage wave sources have an electric equivalent. The basic steps of the demonstration are graphically represented in Fig. 10(a); the equivalence follows from the properties of rows 3 and 4 of Table II. The electric equivalent can be used to find how a given voltage wave source changes when the reference impedance defining the voltage waves is varied, as it is shown by the sequence in Fig. 10(b). The equivalence of Fig. 10(b) allows us to obtain the source terms for the nonmatched characteristics from the sources of the matched characteristics, that are much easier to compute.

ACKNOWLEDGMENT

REFERENCES

[1] C. D. Taylor, R. S. Satterwhite, and C. W. Harrison, Jr., "The response of a terminated two wire transmission line excited by a nonuniform electromagnetic field," *IEEE Trans. Antennas Propag.*, vol. AP-13, pp. 987–989, Nov. 1965.
[2] C. R. Paul, "Frequency response of multiconductor transmission lines illuminated by an electromagnetic field," *IEEE Trans. Electroman. Compat.*, vol. EMC-18, pp. 183–190, Nov. 1976.
[3] A. K. Agrawal, H. J. Price, and S. H. Gurbaxani, "Transient response of multiconductor transmission lines excited by a nonuniform electromagnetic field," *IEEE Trans. Electroman. Compat.*, vol. EMC-22, pp. 119–129, May 1980.
[4] F. Rachidi, "Formulation of field to transmission line coupling equations in terms of magnetic excitation field," *IEEE Trans. Electroman. Compat.*, vol. 35, pp. 404–407, Aug. 1993.
[5] S. Pignari and F. G. Canavero, "EMC analysis and prediction of complex electronic systems," *Int. J. Electron.*, vol. 74, pp. 615–625, 1993.
[6] J. E. Schutt-Aine and R. Mittra, "Nonlinear transient analysis of coupled transmission lines," *IEEE Trans. Circuits Syst.*, vol. 36, pp. 959–967, July 1989.
[7] J. E. Schutt-Aine "Transient analysis of nonuniform transmission lines," *IEEE Trans. Circuits Syst.*, vol. 39, pp. 378–385, May 1992.
[8] T. Dhaene, L. Martens, and D. De Zutter, "Transient simulation of arbitrary nonuniform interconnection structures characterized by scattering parameters," *IEEE Trans. Circuits Syst.*, vol. 39, pp. 928–937, Nov. 1992.
[9] I. Maio, S. Pignari, and F. G. Canavero, "Influence of the line characterization on the transient analysis of nonlinearly loaded lossy transmission lines," *IEEE Trans. Circuits Syst.*, vol. 41, pp. 197–209, Mar. 1995.
[10] R. E. Collin, *Foundations for Microwave Engineering.* New York: McGraw-Hill, 1992, ch. 4.
[11] F. M. Tesche, "Plane wave coupling to cables," in *Handbook of Electromagnetic Compatibility.* San Diego: Academic Press, 1994.
[12] F. Canavero, V. Daniele, and R. Graglia, "Electromagnetic pulse interaction with multiconductor transmission lines," *Electromagn.*, vol. 8, pp. 293–310, Aug. 1988.
[13] J. E. Schutt-Aine and R. Mittra, "Scattering parameters transient analysis of transmission lines loaded with nonlinear terminations," *IEEE Trans. Microwave Theory Technol.*, vol. MTT-36, pp. 529–536, Mar. 1988.
[14] I. Maio and F. G. Canavero, "Lossy transmission line response via numerical Laplace Transform inversion," in *ISCAS 1994 Proc.*, vol. 6, June 1994, pp. 133–135.
[15] Eo and W. R. Einsenstadt, "High-speed VLSI interconnect modeling based on S-parameter measurements," *IEEE Trans. Components, Hybrids, Manufacturing Technol.*, vol. 16, pp. 555–562, Aug. 1993.
[16] R. K. Hoffmann, *Handbook of Microwave Integrated Circuits.* Artech House, 1987, ch 6.
[17] T. Komuro, "Time-domain analysis of lossy transmission lines with arbitrary terminal networks," *IEEE Trans. Circuits Syst.*, vol. 38, pp. 1160–1164, Oct. 1991.
[18] T. S. Blazeck and R. Mittra, "Transient analysis of lossy multiconductor transmission lines in nonlinear circuits," *IEEE Trans. Components, Hybrids, Manufacturing Technol.*, vol. 14, pp. 618–627, Sep. 1991.